12th International Symposium on Turbulence and Shear Flow Phenomena (TSFP12)
Osaka, Japan, July 19–22, 2022

SEPARATION CONTROL WITH AIR-JET VORTEX GENERATORS OF SHOCK/BOUNDARY-LAYER INTERACTIONS ON FLEXIBLE PANELS

Anne-Marie Schreyer
Institute of Aerodynamics and Chair of Fluid Mech
RWTH Aachen University
Wüllnerstr. 5a, 52062 Aachen, Germany
a.schreyer@aia.rwth-aachen.de

Deepak Prem Ramaswamy
Institute of Aerodynamics and Chair of Fluid Mech.
RWTH Aachen University
Wüllnerstr. 5a, 52062 Aachen, Germany
d.ramaswamy@aia.rwth-aachen.de

Christopher Julian Schauerte
Institute of Aerodynamics and Chair of Fluid Mechanics
RWTH Aachen University
Wüllnerstr. 5a, 52062 Aachen, Germany
c.schauerte@aia.rwth-aachen.de

ABSTRACT

Shock/turbulent boundary-layer interactions (STBLI) with separation are ubiquitous in aerospace-transportation applications and detrimentally affect the aerodynamic performance and system integrity. We therefore aim to understand the effect of separation control with air-jet vortex generators (AJVGs) on STBLI over both rigid and compliant walls, with the ultimate goal to reduce structural vibrations induced by the low-frequency unsteadiness of the shock system. An experimental study of a 24° compression-ramp interaction at Mach 2.52 over rigid and flexible panels of varying aspect ratio, with and without the influence of an array of AJVGs was carried out. The flow topology, turbulence behavior in the interaction region, and panel-flutter behavior are presented and discussed.

INTRODUCTION

Shock/turbulent-boundary-layer interactions (STBLIs) occur in a variety of external and internal flows in supersonic flight and propulsion. For example, shock waves are generated at compression surfaces in the inlets of air-breathing engines. For strong shocks, the flow separates, which detrimentally affects the engine performance. Related effects include loss of total pressure, inlet instability, locally high thermal loading, and structural fatigue. To the latter, low-frequency motions of the shock/separation-bubble system (see e.g. Clemens & Narayanaswamy (2014)) are particularly relevant. If a resonant frequency of the structure is approached, induced structural vibrations may compromise the structural integrity.

It is therefore of great interest to decrease shock-induced separation and control the shock-oscillation frequency. Small sub-boundary-layer vortex generators, in particular air-jet vortex generators (AJVGs), have shown promising effectiveness on rigid surfaces (see e.g. Ramaswamy & Schreyer (2021)).

As many surfaces and structures in aerospace systems are not rigid, the strong and unsteady aerodynamic loads imposed by STBLIs result in coupled dynamics with compliant surfaces. STBLIs over rigid walls have been extensively studied for several decades (Gaitonde (2015)), but the effects of wall flexibility on the phenomenon have not yet been fully understood, although progress has been made (see e.g. Daub *et al.* (2016); Spottswood *et al.* (2019); Hoy & Bermejo-Moreno (2021)). Also, the response of this coupled system to separation control has not been studied in detail so far.

The objectives of this research are to a) elucidate the fundamental mechanisms of interactions among shock waves, turbulent boundary layers, and the compliant panels over which these STBLI develop, and b) assess the effectiveness of separation control with AJVGs on STBLIs over flexible panels.

An experimental approach, including flow visualizations with a schlieren setup, velocity measurements with particle-image velocimetry (PIV), and digital image correlation (DIC) to study the panel deformation and flutter, is used to analyze this complex fluid-structure interaction (FSI). Here, we present an analysis of the effect of panel aspect ratio and AJVG control on the flow topology, turbulence evolution in the interaction region, and panel-flutter behavior.

EXPERIMENTAL SETUP AND CONDITIONS

The experimental investigations for this study were conducted in the trisonic wind-tunnel facility at RWTH Aachen University. The intermittently-operating vacuum-storage facility achieves stable run times of $3-4$ s. Air as the working fluid is supplied to a settling balloon. To avoid condensation effects, the air is dried and the relative humidity is kept below 6%. The test section has a cross-section of $0.4 \times 0.4\,\mathrm{m}^2$; optical access is provided by two circular windows on either side of the test section and one on the top wall. The ambient conditions in the laboratory set the wind tunnel stagnation conditions; the selected free-stream Mach number of $M_\infty = 2.52$ thus determines the Reynolds number ($Re_\infty = 9.6 \cdot 10^6\,1/m$).

To create a STBLI, a 24°-compression ramp is installed on a flat-plate model (see Fig. 1). The fully turbulent incoming boundary layer has a thickness of $\delta_0 = 10.4\,\mathrm{mm}$ at $x = 4.5\delta_0$ mm upstream of the ramp corner.

A cavity covered by the respective flexible panel is implemented into the flat plate upstream of the ramp corner. The steel panels (AISI 304) have a thickness of $h = 0.15\,\mathrm{mm}$ and a flutter parameter of $\lambda = 509$. Panel widths of 40, 80, and

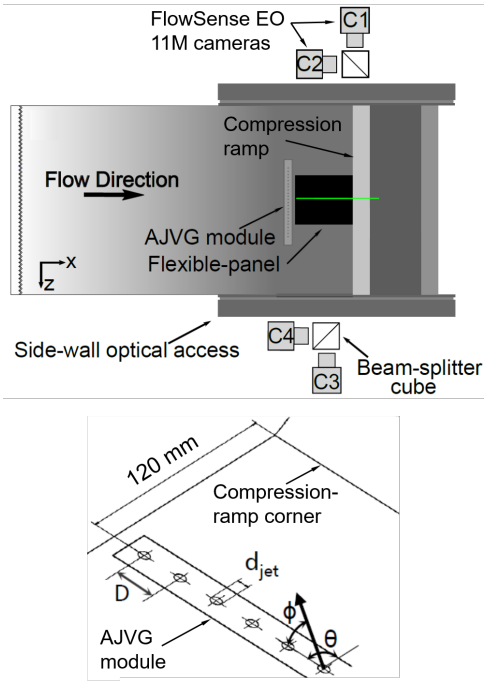

Figure 1. Schematic of the wind-tunnel model and PIV setup (top). Detail view of the AJVG array (bottom).

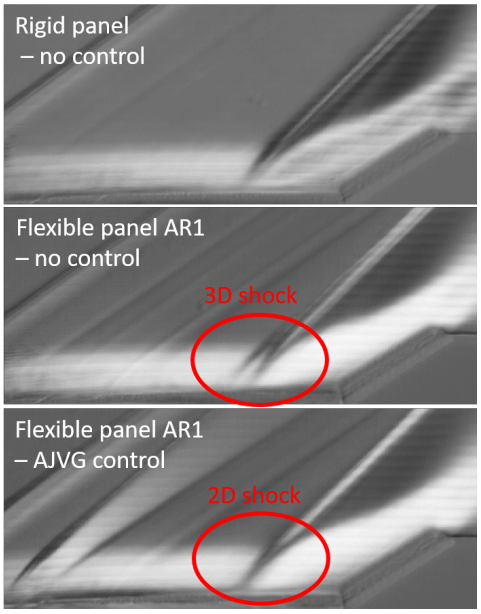

Figure 2. Schlieren visualizations for the rigid panel and AR1 flexible panel without and with control (averaged from 20 instantaneous images; depth of focus: 40 mm).

120 mm at a length of 80 mm create panel aspect ratios of 0.5, 1.0, and 1.5 (cases AR0.5, AR1, and AR1.5, respectively). The upstream and downstream edges of the panels are fixed, both lateral edges are free. The pressure in the cavity is equal to the free-stream static pressure. The panel length was selected such that the compression-ramp-induced shock wave is located approximately along the spanwise flexible-panel center line.

For the control cases, a one-row array of AJVGs (jet-orifice diameter $d_{jet} = 1$ mm, jet spacing $D = 8d_{jet}$, injection angles $\phi = 45°$ and $\theta = 90°$; see Fig. 1) is installed at 120 mm (=$11.5\delta_0$) upstream of the ramp corner. Each jet is injected at a pressure of 1 bar and with a mass-flow rate of 0.0041 kg/s.

Two-component PIV measurements were conducted in the streamwise/wall-normal center plane of the model (equivalent to the location of an AJVG orifice for the control-cases). We used a 527 nm Litron NANO-L pulsed PIV laser with a maximum pulse energy of 200 mJ to illuminate the DEHS seeding particles. Images were recorded with four FlowSense EO 11M cameras (C1 – C4 in Fig. 1), equipped with 4008 px×2672 px CCD sensors and Tamron SP AF 180mm f/3.5 objectives. Two cameras each observed the same field of view (FOV): the first FOV covered the entire flexible-plate region (C3, C4; $-8.8\delta_0 \leq x \leq 1.9\delta_0$), the second FOV covered the STBLI (C1, C2; $-5.8\delta_0 \leq x \leq 4.1\delta_0$). The FOV was split to obtain a sufficiently high spatial resolution (40 px/mm). The respective cameras observing the same FOV were triggered alternately to increase the overall acquisition rate to 10 Hz. PIV measurements are available for the rigid surface, the AR0.5, and AR1.5 flexible panels.

Focusing-schlieren visualizations were carried out with the system described by Schauerte & Schreyer (2018). Images are taken at the model-center plane using a PCO Dimax HS4 high-speed camera at a resolution of 1402 x 502 px and with an exposure time of 2 μs.

For the DIC measurements of the flexible-panel motion, a speckle pattern was applied to the matte-black painted panel surface. A reference image at the rest position of the panel is used for correlations with the oscillating panel. The panel was illuminated continuously with off-the-shelf tungsten light sources and recorded with two Photron SA.5 high-speed cameras setup in stereoscopic configuration. The cameras looked down onto the model from the side at an angle of approximately 30°. Images were recorded with a resolution of 1024 x 640 pixels (9.8 px/mm) at an exposure time of approx. 100 μs.

The schlieren and DIC systems are synchronized using an ILA high-speed synchronizer, recording at 9.3 kHz.

RESULTS

In this article, we present the first analysis of this data set, including a discussion of the flow topology, the evolution of the turbulent velocity field upstream of the ramp corner, and the flexible panel flutter frequency and deflection modes. Both the effects of panel aspect ratio and of separation control with AJVGs are analyzed.

Flow topology

The overall flow topology does not fundamentally differ for STBLIs on rigid and compliant surfaces. A large-scale shock-induced separation forms in the vicinity of the ramp corner (see the flow visualizations in Figs. 2 and 3). In the uncontrolled case (oil-flow visualization for baseline case on a rigid surface; left image in Fig. 3), the separation line is straight and 2D. In the AJVG-controlled case, the overall separation length L_s decreases, and the separation line becomes wavy and spanwise periodic.

The presence of a flexible panel leads to an increase in separation length, with and without control (see Fig. 4; length between extrapolated mean-shock position on the wall and ramp corner in PIV). This increase in separation length is most probably related to 3D effects due to the panel deformation and/or the dynamics of the flow. The shock front in all flexible-panel cases, for example, is 3D even in the uncontrolled case (see double shock foot in focusing schlieren visualization in Fig. 2).

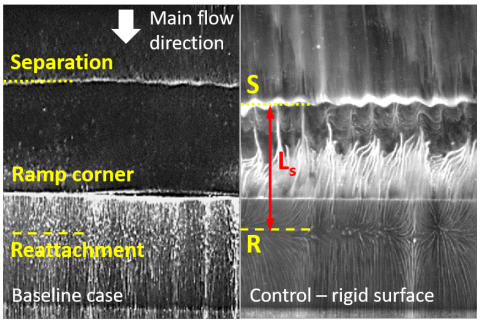

Figure 3. Surface oil-flow visualizations of the STBLI region without and with AJVG control (rigid panel).

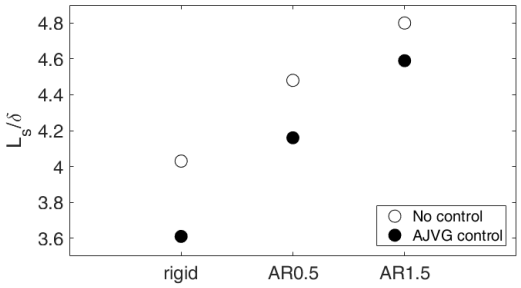

Figure 4. Separation lengths from PIV.

AJVGs successfully reduce the separation length for both the rigid surface and the flexible-panel cases (see Fig. 4). For the compliant wall, the reduction is slightly smaller (7.14%, from 4.48δ to 4.16δ for the AR0.5 case and 4.38%, from 4.8δ to 4.59δ for AR1.5) than for the rigid surface (10.42%, from 4.03δ to 3.61δ), and the control effectiveness decreases with increasing panel aspect ratio. For the compliant wall, AJVGs seem to alleviate 3D effects, as e.g. visible in the shock-foot visualization (Fig. 3 (right)).

Velocity field and turbulence

Figures 5 and 6 show the development of the turbulence intensity of the streamwise (u_{rms}) and wall-normal (v_{rms}) velocity components, respectively, for the rigid surface and the 40 mm and 120 mm flexible panels without (top) and with control (bottom) upstream of the ramp corner. Three influences affect the boundary-layer turbulence: the interaction with the compression ramp, the AJVG control, and the panel flutter due to flexibility of the surface.

For all cases, the turbulence intensity of both components initially increases over the shock. After this initial increase, the u_{rms} remain on a constant level, while the v_{rms} increase further due to streamline-curvature effects. The respective intensity maxima are located within the separation region; towards the boundary layer edge, the turbulence levels decrease to the free-stream/measurement-noise level. Due to the displacement effect of the separation bubble, the maxima shift away from the surface as the ramp corner is approached.

The increase in u_{rms} is stronger for the flexible panels (a factor of 2.9 versus 2.6 for the rigid panel) due to the effect of panel flutter on the boundary-layer turbulence.

Downstream of the separation location, a secondary maximum farther away from the surface can be observed where the profile traverses the shock. This maximum is located farther away from the surface for the compliant wall, and increasingly so with increasing panel aspect ratio – thus indicating the upstream shift of the shock with increasing separation length.

Under the influence of control, the u_{rms} maximum in the separation bubble (weakly) increases further initially, then decreases again slightly, before remaining constant for $x/\delta_0 \geq -2$. The initial increase is higher for the rigid panel (20% at $x/\delta_0 = -3$ vs. 10% for both flexible panels). For the overall u_{rms} after this initial increase, no simple trend regarding the influence of a flexible panel emerges from this preliminary analysis: for the rigid panel, the u_{rms} level returns to the same value as for the uncontrolled case. For the AR1.5 flexible panel, the maximum marginally decreases by 2%, whereas for the AR0.5 flexible panel, a 15% reduction in turbulence intensity is observed for the controlled case. This value is the lowest of all presented cases.

Also for v_{rms}, the overall increase in turbulence intensity across the shock/boundary-layer interaction is larger for the flexible panel cases (factor of 1.8 vs. 1.62 for the rigid surface). Here, an effect of panel aspect ratio can be observed: the overall increase is slower for the low-aspect-ratio panel (AR0.5) than for the AR1.5 panel, i.e. the same overall increase is reached over a longer downstream distance.

Under the influence of AJVG control, the continuous increase in v_{rms} after the initial increase over the shock is slower for the AR0.5 compliant wall, so that at $x/\delta_0 = 0$ an overall decrease in v_{rms} (compared with the uncontrolled case) is observed; the intensity maximum and profile coincide with the rigid-panel case for $x/\delta_0 \geq -2$. For the AR1.5 panel, a higher v_{rms} maximum than in the uncontrolled, rigid and AR0.5 panel cases is reached.

This behavior indicates complex interactions between panel flutter, the separation bubble, the shear layer, and the vortex structures induced by the AJVG control. These interactions are also affected by the panel aspect ratio. To get the full picture, we will analyze the turbulent structures and dynamic mechanisms in more detail in the future. The turbulence behavior probably varies with the spanwise location inbetween the jet orifices, just as for rigid surfaces (see Ramaswamy & Schreyer (2021)). PIV data across the model span would be helpful to study these aspects.

Panel flutter

The induced dominant oscillation frequency of the panel, extracted from DIC measurements at the center location of the respective panels, is indicated in Fig. 7. The frequency is mostly constant along the panel in the streamwise direction and therefore only shown for the one location.

The frequency increases with the aspect ratio of the flexible panel. Under the influence of AJVG control, the frequency decreases. These trends remain, even when normalized with the respective separation lengths (St_L).

The decrease is weakest for the square panel (AR1), where the AJVG control seems to barely affect the induced panel-flutter frequency.

Overall panel displacements of ± 2 mm $= \pm 0.19\delta_0$ are reached during a flutter cycle. The maximum displacements are shown exemplarily for the AR1.5 panel in Fig. 8.

In the uncontrolled baseline state, the deflection is stronger in the $-z$-direction for all tested panel aspect ratios (see Fig. 8 (left) for AR1.5), as one might expect since the pressure fluctuations exerted by the shock impacting the panel from above.

Under the influence of AJVG control, however, the overall deflections become stronger in the $+z$-direction for AR0.5 (not shown) and AR1.5 (Fig. 8 (right)), and almost equally

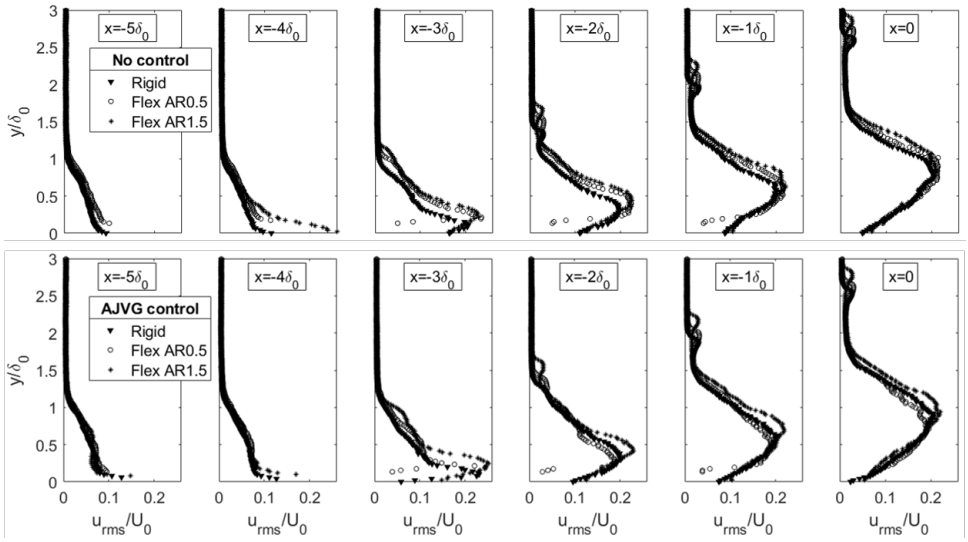

Figure 5. Boundary-layer profiles of the root-mean square of the fluctuating component of the streamwise velocity upstream of the ramp corner ($x/\delta_0 = 0$). Top: no control; bottom: AJVG control.

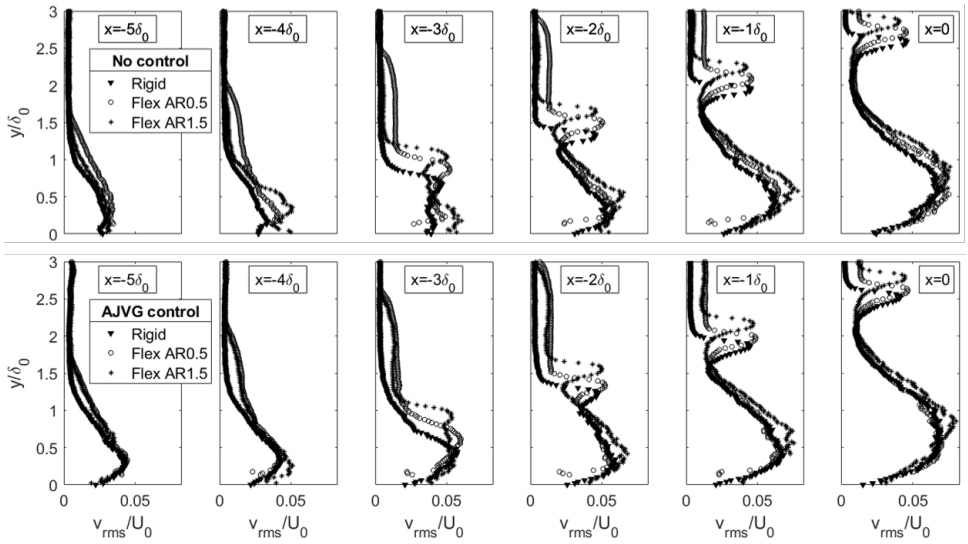

Figure 6. Boundary-layer profiles of the root-mean square of the fluctuating component of the wall-normal velocity upstream of the ramp corner ($x/\delta_0 = 0$). Top: no control; bottom: AJVG control.

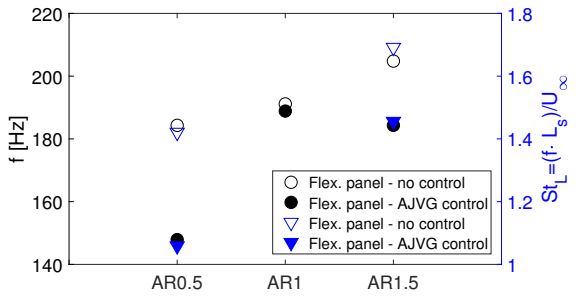

Figure 7. Dominant flutter frequency of the flexible panels.

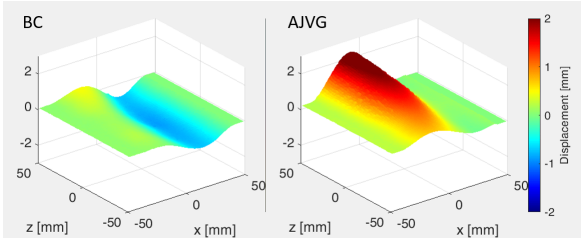

Figure 8. Maximum overall panel deflection for the AR1.5 case. Left: baseline case; right: with AJVG control.

strong in both directions ($\approx \pm 1$ mm) for the square panel (AR1; not shown).

These overall displacements are obtained from superimposing deflection modes.

We analyzed the individual mode shapes associated with the panel displacement during flutter on the basis of a proper-orthogonal decomposition (see e.g. Berkooz *et al.* (1993)) of the DIC measurement data. Based on this decomposition, we intend to clarify how the AJVG control affects the panel-displacement mode shapes and the energy content associated with the respective modes, as well as the influence of panel aspect ratio on this behavior.

The energy content in the respective eigenmodes, as well

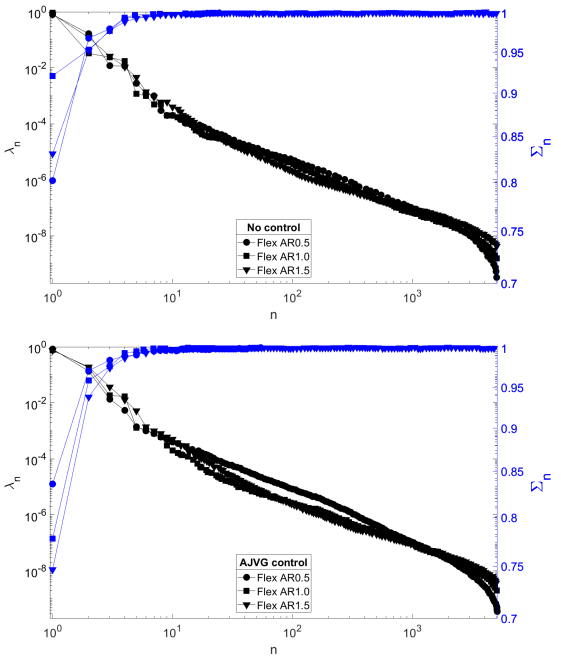

Figure 9. Eigenspectra λ_n and cummulative relative energy $\sum_n$ for the first n POD modes. Left: baseline case; right: with AJVG control.

as the cumulative energy content after a number of n modes is presented in Fig. 9. The eigenmodes are sorted by decreasing fractional energy.

The eigenspectra for all cases show one strongly dominant mode. Without control, this first mode ϕ_1 contains at least 80% of the kinetic energy of the flutter motion, for the AR1 panel even 93%. It can be assumed that this mode corresponds to the extracted dominant panel-oscillation frequency shown in Fig. 7.

Without AJVG control, the largest part of the energy is associated with a panel deflection in the shape of a spanwise valley. For all tested panel aspect ratios, both the first and second modes follow this shape (exemplarily shown for the AR0.5 case in Fig. 10), and further higher modes at lower energy also contribute; for the AR0.5 panel, the fourth and fifth modes have the same shape as modes ϕ_1 and ϕ_2, respectively (not shown), and even the seventh mode ϕ_7 corresponds to a similar type of deflection, although with two peaks and one valley along the streamwise extent of the panel. This shape is to be expected, since the panel flutter is excited by a spanwise oriented shock-wave front moving up- and downstream across the panel's streamwise centerline, and the panel is fixed at both lateral edges.

Two additional mode shapes have weakly significant energy content for the uncontrolled AR0.5 case: ϕ_3, with up- and downwards bent lateral free edges, and ϕ_6, which is symmetric about the panel center point (see Fig.10). Both of these shapes are also among the six most energetic modes for the higher-aspect-ratio panels (not shown).

For AR1 and AR1.5, the larger spanwise spanwise extend enables additional modes including multiple streamwise valleys: ϕ_6 (AR1, see Fig. 11) and ϕ_5 (AR1.5, not shown) with a center peak and downwards bent lateral edges, and modes ϕ_7 and ϕ_8 with a streamwise peak and valley in the center and bent lateral edges for AR1.5 (ϕ_8 shown in Fig.12). These modes, however, have very low energy content (about 0.1%).

The square AR1 panel has an additional interesting set of low energy modes: $\phi_7 - \phi_{10}$ are symmetrical in relation to the diagonal of the panel.

Applying AJVG control to these cases only weakly affects the contributing panel-deflection modes. Modes ϕ_1 and ϕ_2 are still of the same shape as for the uncontrolled case and their energy content amounts to the same total. However, the energy distribution between the modes is modified, as has been expected from the overall deflection shown in Fig. 8.

For cases AR1 and AR1.5, the first mode is slightly less dominant (78% and 75% instead of 93% and 83%, respectively), and more energy is shifted to the second mode ϕ_2 (predominantly) and higher-order modes. This shift in energy is particularly strong for AR1, which agrees with our previously discussed observations of the behavior of the overall deflection, which is almost equally strong in both directions for the square panel (AR1; not shown) under the influence of control. For AR0.5, the opposite happens and the energy content ϕ_1 is weakly increased (compare the top and bottom lines in Fig. 10).

On the basis of the observed dominant panel-deflection modes, we may expect additional spanwise variations in turbulence intensity associated with the panel flutter, in particular for higher aspect ratios. These variations will be superimposed on the spanwise variations associated with AJVG control arrays discussed in the previous section.

CONCLUSIONS

Motivated by the ubiquity of shock/turbulent boundary-layer interactions (STBLI) with separation in aerospace applications, and the detrimental effects of these STBLI on aerodynamic performance and system integrity, we studied the effect of separation control with air-jet vortex generators (AJVGs) on STBLI over both rigid and compliant walls. An experimental study of a 24° compression-ramp interaction at Mach 2.52 over rigid and flexible panels of varying aspect ratio, with and without the influence of an array of AJVGs was carried out.

This article presents the flow topology, development of turbulence in the interaction region, and panel-flutter behavior.

Both the topology and flutter behavior are qualitatively similar for all cases; neither the panel aspect ratio nor the separation control fundamentally change the overall flow and the shapes of the dominant deflection modes of the panel.

However, important details of the flow vary with panel aspect ratio, in particular when interacting with AJVG control.

The separation length and the turbulence amplification across the STBLI increase for compliant surfaces. The turbulence behavior probably also varies more strongly in the spanwise direction, since the effect of panel flutter is added to the influence of spanwise location in relation to the AJVG orifices.

One strongly dominant panel-deflection mode was identified for all cases; the mode corresponds to a panel deflection in the shape of a spanwise valley. The associated panel-flutter frequency increases with the aspect ratio of the flexible panel.

AJVG arrays to control shock-induced separation are almost equally effective on compliant walls as on rigid surfaces – and even more necessary, since larger separation zones are induced due to the interaction between the STBLI and the panel flutter. The reduction in separation length with AJVG control decreases with increasing panel aspect ratio. Also the reduction in turbulence intensity under the influence of control varies with aspect ratio (stronger decrease for smaller aspect ratio), as does the energy distribution between the deflection modes.

The overall behavior for square panels weakly deviates

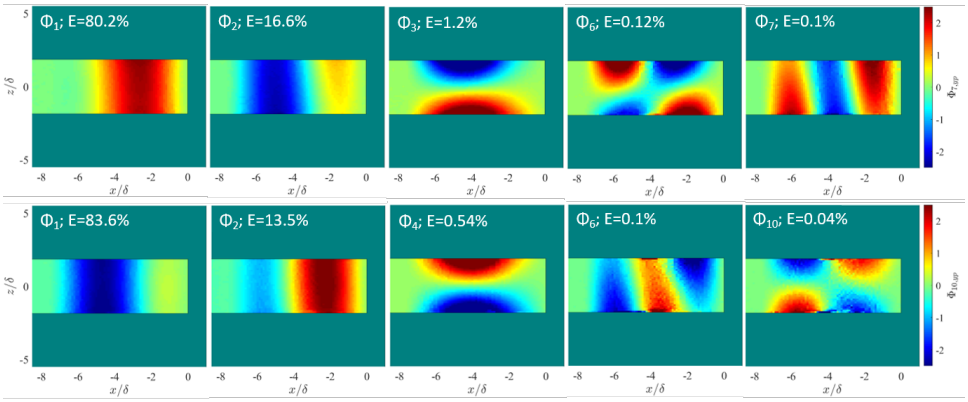

Figure 10. POD modes with the largest energy content for the AR0.5 panel. First row: baseline case; second row: with AJVG control.

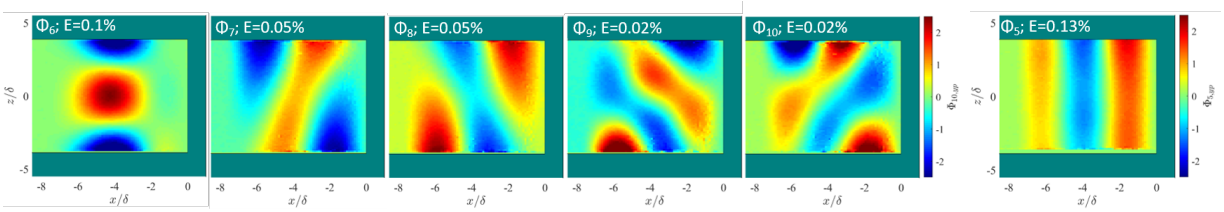

Figure 11. Additional higher-order POD modes for the AR1 panel, which differ from the AR0.5 modes. Five images on the left: baseline case. Image on the right: with AJVG control.

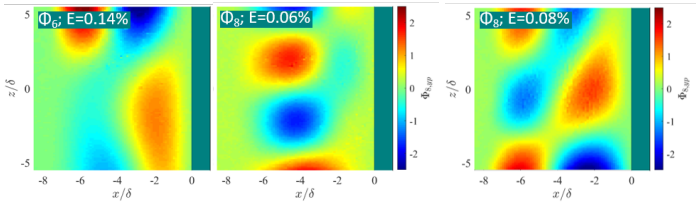

Figure 12. Additional higher-order POD modes for the AR1.5 panel, which differ from the AR0.5 and AR1 modes. Two images on the left: baseline case. Image on the right: with AJVG control.

from rectangular panels: the AJVG control seems to barely affect the flutter frequency and additional deflection modes (symmetric in relation to the panel diagonal) are superimposed. Without control, the first deflection mode for the AR1 panel has an even higher energy content than for the rectangular panels; this difference is mitigated by the AJVG control.

A more detailed analysis of the turbulent structures and dynamic mechanisms will be carried out to explain these observed differences. Overall, the gained knowledge and understanding will allow for the development of effective control setups to mitigate threats to the structural integrity of aerospace applications that are imposed by shock-induced separation.

Acknowledgements

This research was funded by the German Research Foundation (DFG) in the framework of the Emmy Noether grant “Separation Control with Air Jet Vortex Generator Arrays in Transonic and Supersonic Flow” (grant 326485414).

REFERENCES

Berkooz, G., Holmes, P. & Lumley, J. L. 1993 The proper orthogonal decomposition in the analysis of turbulent flows. *Annual Review of Fluid Mechanics* **25**, 539–575.

Clemens, N. T. & Narayanaswamy, V. 2014 Low-frequency unsteadiness of shock wave/turbulent boundary layer interactions. *Annual Review of Fluid Mechanics* **46**, 469–492.

Daub, D., Willems, S. & Gülhan, A. 2016 Experiments on the interaction of a fast-moving shock with an elastic panel. *AIAA Journal* **54** (2), 670–678.

Gaitonde, D. V. 2015 Progress in shock wave/boundary layer interactions. *Progress in Aerospace Sciences* **72**, 80–99.

Hoy, J. F. & Bermejo-Moreno, I. 2021 Numerical study of STBLI on flexible panels with wall-modeled LES. In *AIAA Scitech Forum*.

Ramaswamy, D. P. & Schreyer, A.-M. 2021 Control of shock-induced separation of a turbulent boundary layer using air-jet vortex generators. *AIAA Journal* **59** (3), 927–939.

Schauerte, C. & Schreyer, A.-M. 2018 Design of a high-speed focusing schlieren system for complex three-dimensional flows. In *Proceedings of the 5th International Conference on Experimental Fluid Mechanics*, pp. 232–237.

Spottswood, S. M., Beberniss, T. J., Eason, T. G., Perez, R. A., Donbar, J. M., Ehrhardt, D. A. & Riley, Z. B. 2019 Exploring the response of a thin, flexible panel to shock-turbulent boundary-layer interactions. *Journal of Sound and Vibration* **443**, 74–89.